Available online at www.sciencedirect.com
SCIENCE DIRECT®
International Journal of Heat and Mass Transfer 47 (2004) 2365–2377
International Journal of HEAT and MASS TRANSFER
www.elsevier.com/locate/ijhmt

Pressure drop and heat transfer analysis of flow boiling in a minichannel: influence of the inlet condition on two-phase flow stability

D. Brutin *, L. Tadrist

Laboratoire I.U.S.T.I., Ecole Polytechnique Universitaire de Marseille, Technopôle de Château-Gombert, 5, rue Enrico Fermi, 13453 Marseille, France

Received 27 June 2003

Abstract

We study flow boiling in a rectangular minichannel of 0.5×4 mm^2 cross-section (hydraulic diameter: 889 μm). A two-phase flow pressure drop analysis by ranging several mass flow rates for a chosen heat flux provided to the minichannel has been performed. Two kinds of upstream conditions have been investigated to show up the confinement influence on boiling. Steady and unsteady thermo-hydraulic behaviors are reported. A stability criterion is found depending on the two controlled parameters (heat flux and mass-flow rate). The upstream condition is modified by adding a compliant buffer tank and the procedure is repeated. Unsteady flows are observed with a different intensity and with a different range of operating conditions when the flow is mainly vapor. When no compliance source is connected, the unsteady behaviors are observed in the same operating conditions. Nevertheless the characteristics of the fluctuations differ notably in amplitude and frequency. In the steady state conditions a pressure loss model is proposed based on a homogeneous assumption. A total pressure loss steady state modeling of the boiling flow is realized using a homogeneous model for the two-phase flow zone to check the steady average minichannel pressure loss. A good agreement is found with the experimental and model results.

PACS: 44.35.+c; 47.27.Te; 47.60.+i
Keywords: Flow boiling; Minichannel; Forced convection; Flow stability

1. Introduction

When boiling occurs in a duct, fluid pressure and temperature behaviors are strongly modified due to the fluid flow state. For industrial applications, the flow stability is needed and found for specific operating conditions. When boiling is investigated in a research area, steady and unsteady states may be observed depending on the controlled parameters. Recent industrial developments of micro-systems (micro-heat-exchanger, micro-fluid-heater, micro-reactors) imply a focus of research on micro-heat and mass transfer in confined geometries. In such small spaces, interfacial phenomena which are often negligible in classical flows become dominant. When a liquid–vapor phase change occurs in a small hydraulic diameter minichannel, the wall proximity may influence the bubble growth and its evolution. On convective boiling in microminichannels limited studies exist. This field is at present under investigation [1,2]. Wen et al. [3] investigated water flow boiling in a minichannel of 1.33 mm and observed wall temperature excursions. They explained this behavior by transient dryout due to the two-phase flow structure of vapor plug and liquid film boiling cooled down by liquid slugs.

* Corresponding author. Tel.: +33-4-91-106868; fax: +33-4-91-106969.
E-mail address: david.brutin@polytech.univ-mrs.fr (D. Brutin).

0017-9310/$ - see front matter © 2003 Elsevier Ltd. All rights reserved.
doi:10.1016/j.ijheatmasstransfer.2003.11.007

Nomenclature

A	area (m^2)
Bi	Biot number (–)
Co	confinement number (–)
C_p	heat capacity ($J\,kg^{-1}\,K^{-1}$)
d	width (m)
D_H	hydraulic diameter (m)
e	thickness (m)
F	frequency (Hz)
h	heat transfer coefficient ($W\,m^{-2}\,K^{-1}$)
L	length (m)
L_V	latent heat of vaporization ($J\,kg^{-1}$)
N_{pch}	phase change number (–)
N_{sub}	subcooling number (–)
P	pressure (Pa)
Po	Poiseuille number (–)
Re	Reynolds number (–)
S	slip ratio (–)
U	velocity ($m\,s^{-1}$)
T	temperature (°C)
z	axial distance (m)

Greek symbols

α	void fraction (–)
χ	vapor quality (–)
Δ	difference (–)
λ	friction factor (–)
μ	dynamic viscosity (Pa s)
ϱ	density ($kg\,m^{-3}$)
σ	surface tension ($N\,m^{-1}$)

Subscripts and superscripts

C	critical
out	outlet
in	inlet
L	liquid
SAT	saturation
TP	two-phase
V	vapor

Many types of instabilities can develop in flow boiling: flow excursion is the most common one explained in a classical minichannel diameter by the Ledinegg criterion [4]. Kew and Cornwell [5] highlighted an appearance threshold of the instability phenomena when the starting diameter of the bubble approaches the hydraulic diameter of the minichannel. The authors proposed a model of pressure fluctuation within cylindrical minichannels, based on the displacement of a liquid slug surrounded by expanding vapor [6]. In 1998, Aligoodarz et al. [7] observed temperature fluctuations of the same order as the average overheating of the wall in minichannels of various sizes. Wang and Peng [8] conducted single-phase and flow boiling experiments of some fluids and mixtures in rectangular microminichannels of hydraulic diameter from 343 to 133 μm and triangular microminichannels ranging from 600 to 200 μm. Unusual phase-change transport phenomena were observed by the authors. They tried to explain such behavior through two new concepts of "evaporating space" and "fictitious boiling". They deduced from their experiments that "nucleate boiling in microminichannels having dimensions from several hundred to less than one micrometer is almost impossible". Jiang and coworkers [9] devised a transparent microminichannel heat sink system to visualize the flow pattern and take temperature measurements during flow boiling. For the low power supplied to the fluid flow, they observed that local nucleation was possible but difficult to generate even for 40 μm hydraulic diameter minichannels. For intermediate power, slug flows develop and for a high power supply a steady annular flow mode is noticed. Yu et al. [10] realized single and two-phase flow experiments in microtube diameters of 19, 52 and 102 μm. For a laminar flow, they observed a lower value of Poiseuille number ($Po = \lambda Re$) of 53 instead of 64 and a similar lower behavior for a turbulent one. The experimental Nusselt number was also enhanced to compare with the predicted values. To our knowledge, the influence of upstream and downstream conditions on flow boiling stability have rarely been studied.

In a previous study, in which we realized flow visualization in a minichannel, we showed up the confinement effect on two-phase flow behavior [11]. Typical unsteady cases were detailed with pressure measurement analysis. It was evidenced that when unsteady behavior is observed with a compliant source connected, a back two-phase flow to the entrance may appear. Without a compliance source connected the flow visualization indicated a liquid–vapor film flow coupled with two-phase plug expulsion.

The aim of this paper is to analyze the stability range and two-phase flow behaviors for two different upstream conditions: when a damper is introduced upstream to the minichannel coupling with the loop can appear. The fluid flow is temporally stored in the compressible volume (damper) when the minichannel pressure loss is too high and when the pressure in the buffer is higher than the minichannel pressure loss, the fluid is re-injected. A constant mass flow rate condition is considered before the buffer whereas for the case without a buffer connected, no coupling is possible and a constant mass flow

rate is provided to the minichannel entrance. The objective is to acquire better knowledge of the boundary conditions' influence on the two-phase flow and heat transfer in the minichannel. The two-phase flow stability will be analyzed through pressure loss versus inlet mass flow rates for different heat fluxes supplied to the minichannel. An analysis of the experimental results is presented and non-dimensional pressure loss and heat transfer laws are derived for both inlet flow conditions.

2. Experimental set-up

We briefly remind you in this paper the main components of the loop and the new developments realized. The experimental setup has been fully detailed in a previous study [11]. The main component of the loop is a minichannel heated through the back and the lateral sides. The fluid (*n*-pentane) flows vertically upward (Figs. 1 and 2). A compressible volume (buffer tank) is realized using a 400 mm-long and 30 mm-diameter rigid polycarbonate® tube. The buffer tank containing a given volume of *n*-pentane is connected to the loop before the minichannel entrance using a valve.

The fluid contained in the loop is boiled for several minutes to eliminate the non-condensable gas through a valve opening in the loop. The experiments are then carried out using a given procedure: for a fixed heat flux and mass flow rate, the fluid entering the minichannel is heated. Depending on the experiment's controlled parameters, several zones may be observed in the minichannel (liquid, two-phase, vapor). Temperature and pressure measurements are permanently acquired at different scanning frequencies (100–500 Hz) according to the observed phenomena's dynamics. The heating power is stepped up then a new experiment is investigated. All acquired data are post-processed. When the stationary state is reached for each running condition (mass flow rate, heat flux) the time averages of temperature and pressure are calculated. The vapor quality, the pressure drop and the local superheating are deduced. The dynamics of the parameters are then analyzed (temperature and pressure). For each experimental condition, the frequency and amplitude fluctuations are deduced.

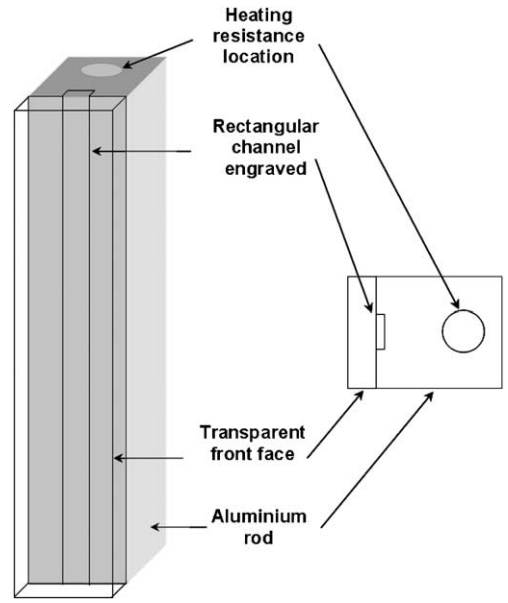

Fig. 2. Diagram of the engraved minichannel (front view on the left and top view on the right).

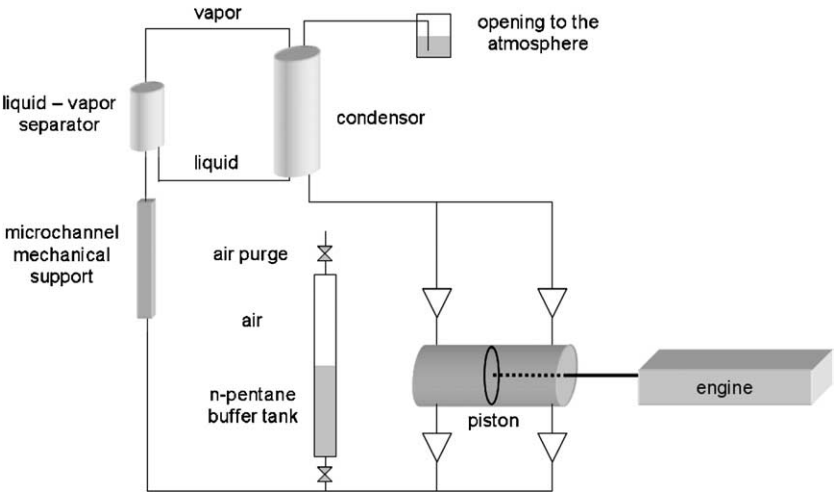

Fig. 1. Experimental set-up designed for two-phase flow stability investigations.

3. Pressure loss variations

3.1. Typical pressure variations

In Fig. 3 the pressure drop is presented versus the inlet Reynolds number (Re_{IN}) for a supplied heat flux of 89.9 kW m^{-2}. The inlet temperature is the room temperature (25 °C) and the outlet pressure is kept constant at atmospheric pressure. The provided mass flow rate is constant at the minichannel entrance. These conditions corresponding to a subcooled liquid are maintained constant for all the experiment duration. An N-shaped curve is found.

Before point C of Fig. 3, that is for Reynolds numbers lower than 2000, the pressure drop increases as Re_{IN} increases. In addition, for inlet Reynolds numbers lower than 1500, pressure fluctuations appear. In the range of 250–6500, two zones exist in the minichannel: a liquid and a two-phase one. The length of each zone varies in accordance with Re_{IN}. The two-phase zone is larger for $Re_{IN} = 1500$ at point D while the liquid one is smaller. On the contrary the liquid zone is larger for $Re_{IN} > 6500$ at point A. For Re_{IN} lower than 250, that is before point E, a vapor zone appears near the minichannel exit. It invades the minichannel as Re_{IN} decreases. In the range of 0–250, three zones (liquid, two-phase and vapor) coexist in the minichannel.

3.2. Modeling

To analyze the previous experimental pressure loss variation, a one-dimensional model is developed. The physical parameters for the model are listed in Table 1 for a numerical application. Let us consider an electrical power provided to the minichannel from 125.6 to 15.7 W. It gives a heat flux from 125.6 to 15.7 kW m^{-2}. The model takes into account the existence of three possible zones depending on the controlled parameters and the physical properties of the fluid. The detailed model is presented in Appendix A. In Fig. 3 the experimental pressure loss and model results are presented. A good agreement between the experimental and calculated pressure loss is found. The N-shaped curve is also described with the one-dimensional model in the steady state regime. For Reynolds numbers lower than 1500, the non-steady regime appears. The present model is no longer relevant for this regime due to the steady state assumption.

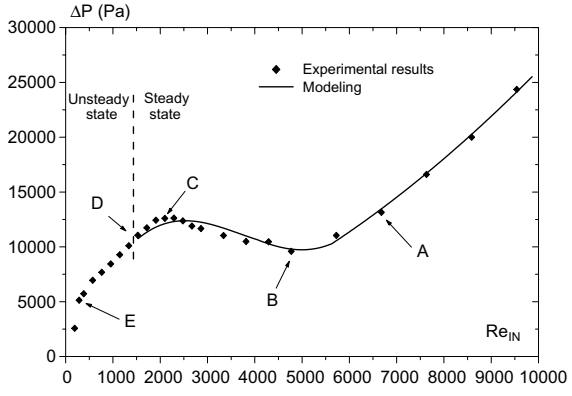

Fig. 3. Average pressure loss versus inlet liquid Reynolds number for a heat flux of 89.9 kW m^{-2}.

Table 1
n-Pentane liquid and vapor physical properties

Conditions		Value	Unit
25 °C	σ	13.12×10^{-3}	N m^{-1}
25 °C	μ_L	2.23×10^{-4}	Pa s
	ϱ_L	621	kg m^{-3}
	C_{P_L}	2142	J kg^{-1} K^{-1}
36 °C	ϱ_V	2.57	kg m^{-3}
	μ_V	6.78×10^{-6}	Pa s
	C_{P_V}	1717	J kg^{-1} K^{-1}
1010 hPa	T_{SAT}	36	°C
36 °C	L_V	382,450	J kg^{-1}

3.3. Two-phase flow pressure loss analysis

From the proposed model, the conditions of the several effects on the pressure loss are analyzed in the two-phase zone. In Fig. 4, the pressure loss for the liquid and two-phase zones are presented versus Re_{IN}. Moreover, the corresponding total pressure loss is presented. As Re_{IN} increases the conditions of the liquid pressure loss become significant while the two-phase flow pressure loss decreases. The two-phase zone vanishes for inlet Reynolds numbers higher than 5400. In the two-phase zone, the pressure loss is due to three effects (gravity, acceleration and friction). The main effect on the pressure loss is that of friction. The acceleration is five times less while the gravity effect is negligible whatever the inlet Reynolds number considered.

3.4. Influence of the heat flux

We investigated the pressure loss versus the inlet liquid Reynolds number for five heat fluxes. The minichannel pressure loss measured is plotted as a function of the inlet Reynolds number in Fig. 5. The same N-shape behavior is observed whatever the imposed heat flux. As the heat flux is increased, the pressure loss is shifted for higher values and the N-shaped curve is more and more pronounced. The steady and unsteady regimes exist for all the imposed heat fluxes. The dark points correspond to the steady state regime whereas the white ones correspond to the unsteady regime.

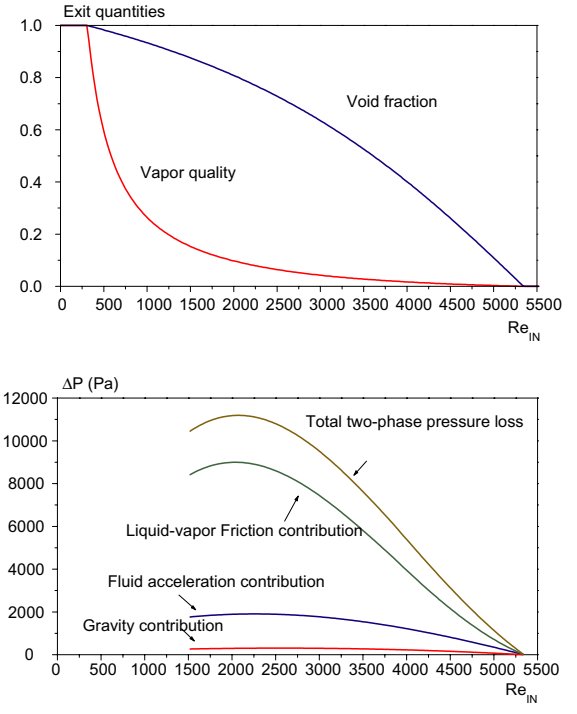

Fig. 4. Sum of all contributions to the two-phase pressure loss (friction, acceleration and gravity) for heat flux of 89.9 kW m^{-2} and exit quantities (vapor quality and void fraction).

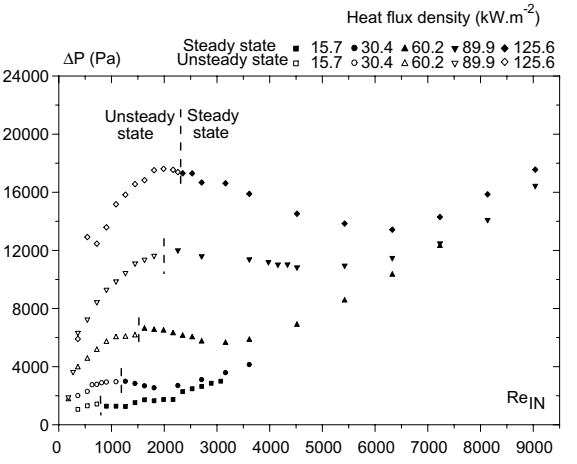

Fig. 5. Average pressure loss versus inlet Reynolds number when the buffer is not connected to the loop for five heat fluxes.

4. Influence of the inlet condition

The two-phase flow stability is generally influenced by the boundary conditions. These conditions have seldom been investigated in the literature. Preliminary experiments indicated a strong dependence of the boundary conditions on the thermo-hydraulic behavior in the minichannel [12]. In the present paper, we investigated two different inlet conditions. The first one corresponds to the constant liquid velocity at the minichannel entrance which will be called the confinement case. The second corresponds to a constant velocity at the syringe outlet. Between the syringe and the minichannel a compressible buffer tank is introduced; this case will be called the compliant case. This configuration simulates common cases where compliant tubes or elements exist in two-phase loops. The thermo-hydraulic characteristics are determined for these two cases.

4.1. Compliant case

In Fig. 6, the pressure loss variation versus the inlet Reynolds number is presented for several heat fluxes when the buffer tank is connected. The same N-shaped behavior is observed. Similar results of the average pressure loss are evidenced for the steady state regime. However, for the unsteady state regime, the two-phase flow dynamics is clearly different. This will be detailed in a further section.

The unsteady behaviors are mainly found to be in the range where the pressure drop increases with the inlet Reynolds numbers. The unsteady behavior points confirmed by spectral analysis of the pressure drop signal are reported. Two typical pressure drop variations are presented in Fig. 7a and Fig. 8a for Reynolds numbers of 1336 and 382 respectively, with a same heat flux (125.6 kW m^{-2}). Only the fluctuating component of the pressure loss signal is presented. In Fig. 7a for $Re_{IN} = 1336$ the inlet and outlet pressure signals fluctuate at 3.8 Hz with an average oscillation amplitude of 11

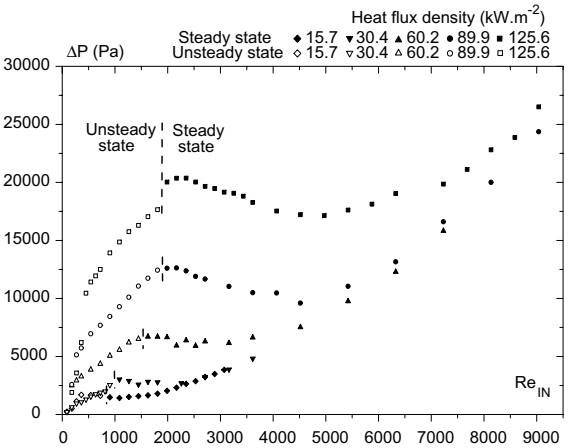

Fig. 6. Average pressure loss versus inlet Reynolds number when the buffer is connected to the loop for five heat fluxes.

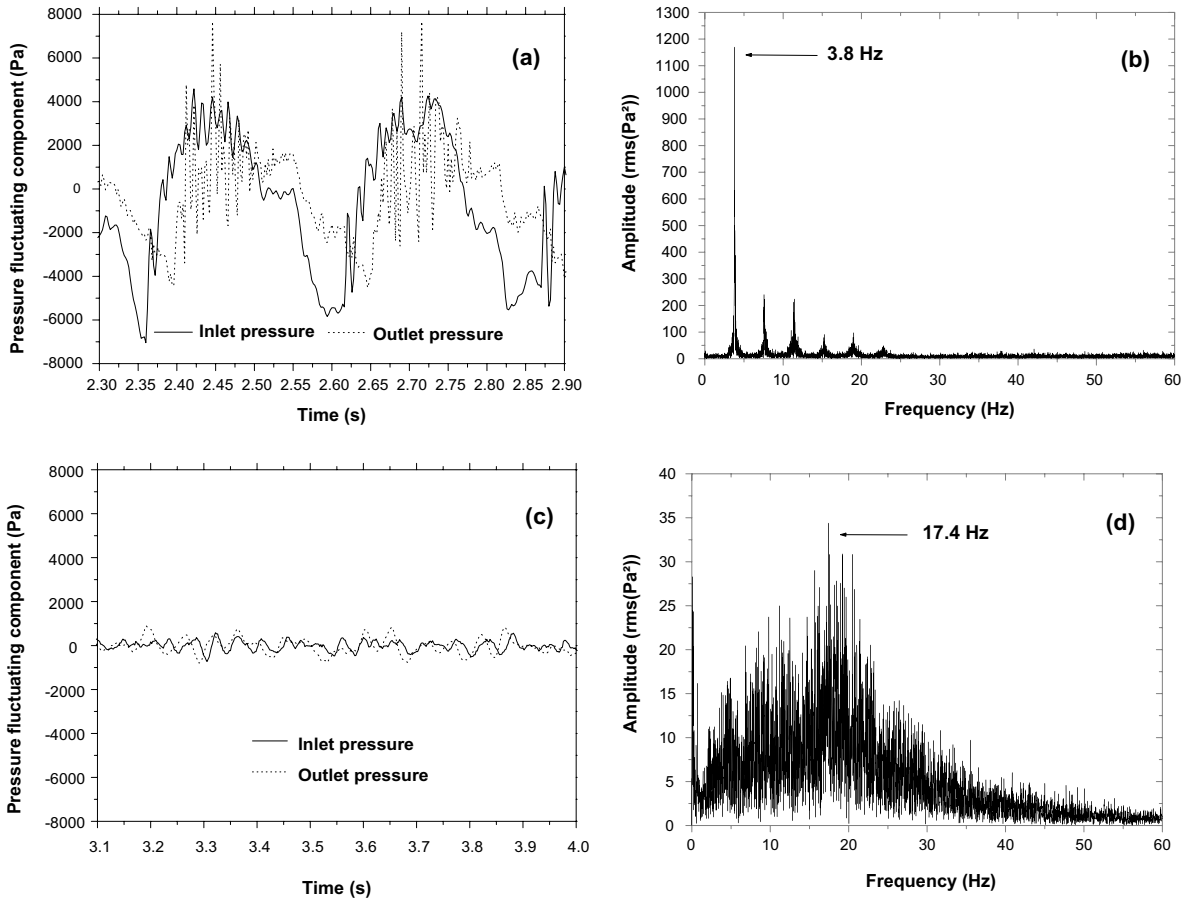

Fig. 7. Inlet and outlet pressure evolution with (a) BT connected and (c) BT not connected. Average pressure drop FFT with (b) BT connected and (d) BT not connected ($Re_{IN} = 1336$ and $Q_W = 125.6\ kW\,m^{-2}$).

kPa. For $Re_{IN} = 382$, the signal evolves as a chugging flow at 4 Hz. Pressure peaks in the pressure signal reach 45 kPa. The main differences between these two behaviors are an oscillating flow around the average pressure loss and a chugging flow with pressure peaks up to 10 times the average pressure loss.

By means of a fast camera analysis at 1000 frames per second of the two-phase flow in the minichannel a specific unsteady behavior was observed for the case: $Re = 1336$. Liquid flows in the minichannel. Bubbles are created at the beginning of the two-phase flow zone. Their size and generation rates are such that bubbles coalesce to vapor slugs which evolve in the minichannel. Vapor slugs generate over-pressure which reduces the upstream boiling flow rate. Bubbles growing before the vapor slug slow down, stop and quickly reach the entire minichannel cross-section. Vapor created by bubble expansion must be evacuated; but downstream in the minichannel vapor slugs block the flow. Expanding vapor pushes the inflow back to the entrance using the buffer tank as a mass flow storage. Finally the minichannel is full of vapor. The surface temperature rises due to the heat flux permanently provided to the fluid and not removed by boiling. When the minichannel is empty and upstream pressure before the minichannel entrance is sufficient, the entire vapor slug which occupies the minichannel is expelled. The minichannel is refilled with liquid. Due to the high surface temperature, bubbles are quickly formed and the phenomenon is repeated.

4.2. Confinement case

Without a buffer tank, the mass flux at the bottom of the minichannel is provided constantly. Also, two behaviors may be observed according to the operating conditions. For increasing inlet Reynolds numbers, when the maximum pressure loss exceeds a critical Reynolds number a steady behavior is observed. For lower Reynolds numbers, an unsteady behavior is also

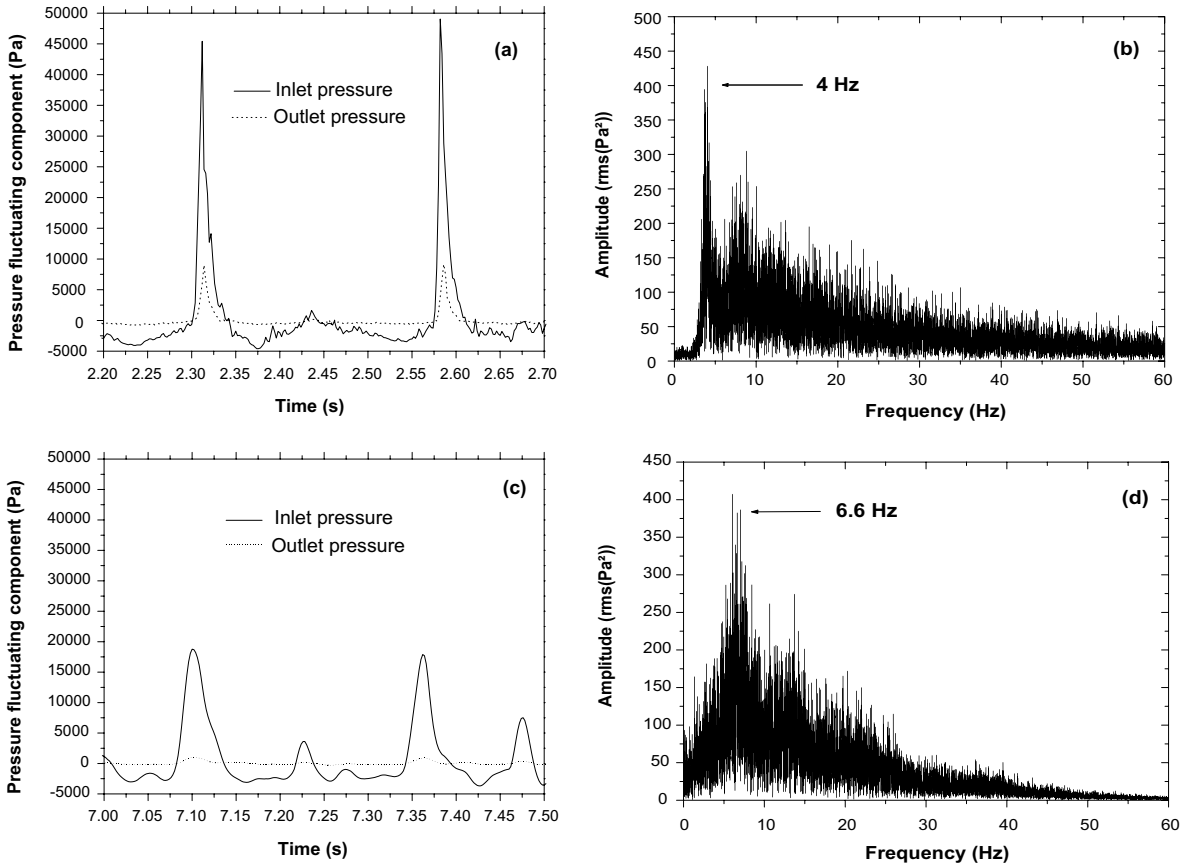

Fig. 8. Inlet and outlet pressure evolution with (a) BT connected and (c) BT not connected. Average pressure drop FFT with (b) BT connected and (d) BT not connected ($Re_{IN} = 382$ and $Q_W = 125.6\ kW\,m^{-2}$).

found as we observed for the previous case. Typical signals are presented in Fig. 7c for a Reynolds number of 1336 and in Fig. 8c for a Reynolds number of 382. For both cases the same heat flux is applied (125.6 $kW\,m^{-2}$). The pressure loss fluctuates at a high frequency 17.4 Hz with a small average fluctuation amplitude 1.6 kPa when the inlet Reynolds number is high ($Re = 1336$) whereas with a lower Reynolds number ($Re = 382$), the pressure loss fluctuates at 6.6 Hz with a fluctuation amplitude of 20 kPa which is not centered on the average pressure loss. All the pressure characteristics are summarized in Table 2.

By means of a fast camera analysis at 1000 frames per second two-phase flow behavior was observed for the case: $Re = 382$. It is composed of a liquid–vapor film flow with liquid plugs which evolve and vaporize in the minichannel. A film flow is established, liquid plugs are formed at the entrance and evolve. The plug formation and evolution induce a pressure loss increase. During their evolution in the minichannel, the plug vapor quality increases, so the pressure loss decreases. When the last plug is virtually vapor, the minichannel pressure loss is minimum and the film flow occupies all the minichannel until the following plug forms. The lower vapor flow and liquid film flow average speed are estimated from experimental measurements at the minichannel entrance. We found $U_V = 4.5\ m\,s^{-1}$ and $U_L = 0.46\ m\,s^{-1}$ respectively, so a speed difference $\Delta U = U_V - U_L = 4\ m\,s^{-1}$. A specific study is needed to characterize the flow characteristics.

4.3. Discussion

The average and amplitude values of the pressure loss for the two cases investigated are reported in Table 2. In Fig. 9 two pressure loss variations are presented for a given heat flux (89.9 $kW\,m^{-2}$), with the pressure loss fluctuation for the unsteady flow state. The pressure fluctuation amplitude is clearly higher in the compliance case. The pressure fluctuation amplitude increases with Reynolds numbers decreasing until they reach a maximum which corresponds to an exit vapor quality of 1. For this case (exit vapor quality of 1) such an amplitude is seven times the average minichannel pressure loss

Table 2
Comparison of the average pressure loss (ΔP), the oscillation frequency (F_0) and the oscillation amplitude (δP) for two typical unsteady behaviors (with or without the buffer tank connected)

	Inlet Reynolds number (heat flux: 125.6 kW m^{-2})					
	382			1336		
	ΔP (kPa)	F_0 (Hz)	δP (kPa)	ΔP (kPa)	F_0 (Hz)	δP (kPa)
With compliance	5.2	4	45	9.4	3.8	11
Without compliance	4.5	6.6	20	14.3	17.4	1.6

($\Delta\overline{P} \sim 5$ kPa, $\delta P \sim 33$ kPa). Then the amplitude decreases due to the fact that the minichannel is more and more empty of liquid and a two-phase flow; the fluctuation is only a vapor flow fluctuation and so a low pressure fluctuation. For the case where no compliance source is connected, the pressure loss fluctuation amplitude is smaller compared to the previous situation. The pressure loss fluctuation amplitude maximum is reached for a lower Reynolds number compared with the previous case. The corresponding amplitude, is however, still about seven times the average minichannel pressure loss ($\Delta\overline{P} \sim 2.2$ kPa, $\delta P \sim 14$ kPa).

In a minichannel of a typical diameter of a few millimeters, instabilities have been found to appear in the compliant case for given operating conditions [4,13,14]. In the representation of the total pressure drop versus the inlet Reynolds number, the negative slope part of the curve may be unsteady. However, depending on the operating conditions, we do not observe such unsteady behavior in our experiments.

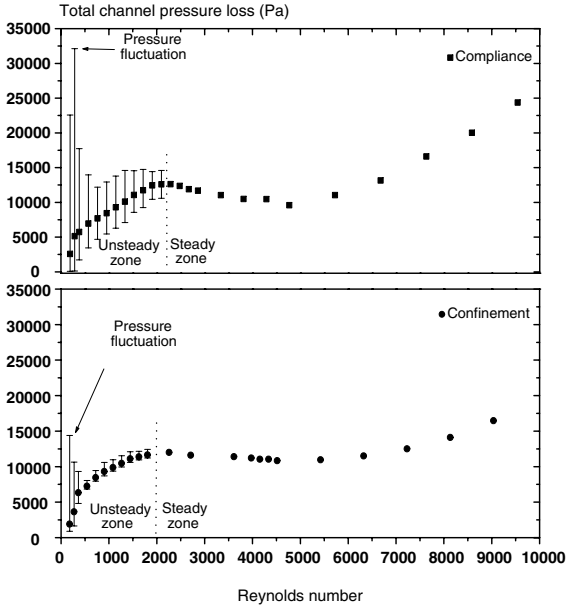

Fig. 9. Comparison between the two upstream conditions of the minichannel pressure loss with the pressure fluctuations ($Q_W = 89.9$ kW m^{-2}).

5. Analysis

5.1. Stability criteria

A stability criterion might be derived from the experimental results considering the two controlled parameters (heat flux and liquid inlet mass flow rate). In both cases previously investigated, instabilities occur in the first increasing part of the curve (Figs. 5 and 6). Whatever the heat flux applied, the unsteady state appears for lower inlet Reynolds numbers compared to the case without compliant upstream conditions. The threshold is lower when a compliance source is inserted in the loop. For all inlet Reynolds number and heat fluxes investigated, the fluctuation amplitudes are much more smaller in the confined case compared to the compliant case. Oscillation frequencies are higher in the compliant case. Furthermore the fast Fourier transform exhibits a characteristic frequency with a narrow band in the second case (Figs. 7b and 8b).

The objective is now to find a common presentation of all the results to summarize all the pressure loss curves obtained experimentally. The pressure loss result will thus be presented non-dimensionally. In the same way, the heat transfer results will be put in non-dimensioned form to be compared. To find the parameter which will allow a comparison between all the experiments, it is necessary to represent the exit vapor quality variation function of the inlet Reynolds number. In Figs. 10 and 11, the experimental results are plotted (χ_{out}: exit vapor quality function of Re_{IN}: inlet Reynolds number). Each curve presents the vapor quality variation versus the inlet liquid Reynolds number for a given heat flux for both upstream conditions. Theses variations can be described by the energy balance equation (1). The exit vapor quality may be deduced assuming a uniform heat flux at the wall.

$$\chi_{out} = \frac{1}{L_V}\left(\frac{4q_W L_H}{\mu Re_L} - \Delta h_i\right) = N_{pch} - N_{sub} \quad (1)$$

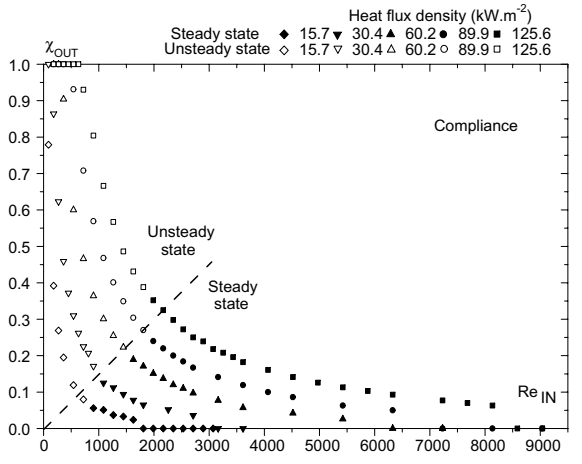

Fig. 10. Exit vapor quality versus inlet Reynolds number for buffer connected to the loop case for five heat fluxes.

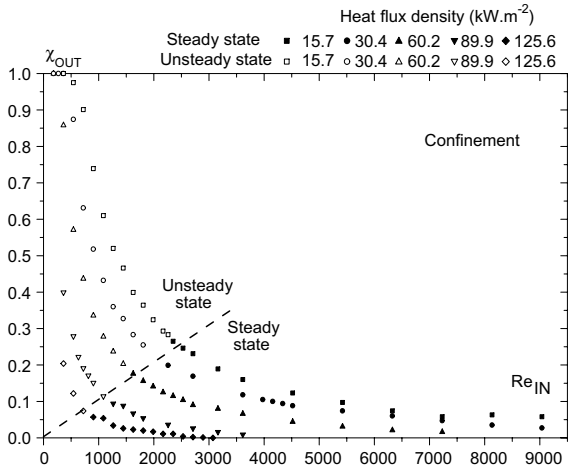

Fig. 11. Exit vapor quality versus inlet Reynolds number for buffer not connected to the loop case for five heat fluxes.

In Fig. 10, for example, the exit vapor quality is plotted versus the inlet Reynolds number. Each curve corresponds to a heat flux investigated.

$$N_{\mathrm{pch}} = \frac{4q_{\mathrm{W}}}{\varrho_0 U_0 L_{\mathrm{V}}} \frac{L_{\mathrm{H}}}{D_{\mathrm{H}}} \tag{2}$$

$$N_{\mathrm{sub}} = \frac{\Delta h_{\mathrm{i}}}{L_{\mathrm{V}}} \tag{3}$$

In Figs. 10 and 11, the critical transition conditions ($\chi^{\mathrm{C}}_{\mathrm{out}}$, Re^{C}) are located by a dash line for all heat fluxes investigated. The characteristic curve of the marginal stability can be evaluated. A linear relation is deduced.

$$\chi^{\mathrm{C}}_{\mathrm{out}} = N^{\mathrm{C}}_{\mathrm{pch}} - N^{\mathrm{C}}_{\mathrm{sub}} = A\,Re^{\mathrm{C}} \tag{4}$$

In Eq. (4) Re^{C} is the critical Reynolds number, $\chi^{\mathrm{C}}_{\mathrm{out}}$ the critical vapor quality and A a constant.

For all Reynolds numbers below this line, boiling is steady whatever the heat flux supplied whereas above this line the boiling flow is unsteady. The flow stability transition is thus observed for a given ratio of $(N^{\mathrm{C}}_{\mathrm{pch}} - N^{\mathrm{C}}_{\mathrm{sub}})/Re^{\mathrm{C}}$. The constant A differs for the two inlet conditions and have been obtained for given parameters such as heated perimeter, cross-section area and fluid. Only experiments can definitively evidence if this stability criteria found is a constant.

5.2. Heat transfer coefficient

The heat transfer coefficient dealt with is the average one using the assumption of a constant heat flux. The heat is provided using an electric resistance element which delivers a constant power and so a constant heat flux to the resistance element ($\overline{Q}_{\mathrm{W}}$). However the heat flux redistributed in the aluminum rod depends on the fluid flow and its states. The local temperature measurements taken cannot be used to obtain a local heat transfer coefficient but provide an average surface temperature and fluid temperature. Using these temperature differences ($\overline{T}_{\mathrm{S}} - \overline{T}_{\mathrm{F}}$), in Fig. 12 we provide the average heat transfer coefficient variation function of the inlet Reynolds number for several heat fluxs as defined by Eq. (5) solely for operating conditions with a two-phase zone in the minichannel to analyze the two-phase heat transfer coefficient variations. In fact, vapor bubbles are created all along the minichannel; this situation corresponds to flow boiling with a subcooled liquid.

$$\bar{h} = \frac{\overline{Q}_{\mathrm{W}}}{\overline{T}_{\mathrm{S}} - \overline{T}_{\mathrm{F}}} \tag{5}$$

Increasing the heat flux the shape of the average heat transfer coefficient is more and more pronounced like

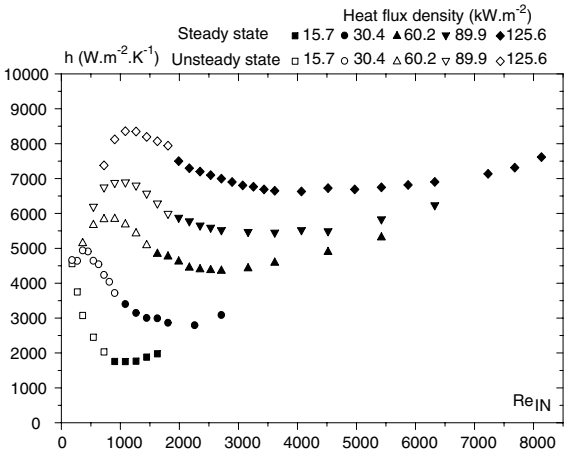

Fig. 12. Heat transfer coefficient for all heat fluxes investigated.

for the pressure loss variation. The dark points in Fig 12 represent the steady state regime whereas the white ones are for the unsteady regime. For the liquid inlet Reynolds number of 8500 and the highest heat flux (125.6 $kW\,m^{-2}$) the flow is liquid and the average heat transfer coefficient is only a forced convection one. For lower Reynolds numbers, a two-phase zone exists and the average heat transfer coefficient decreases to a value of the liquid inlet Reynolds number then increases to reach its maximum. The transition from steady to unsteady state occurs during this increasing part of the curve but does not affect the curve variation. Finally for $Re_{IN} < 1200$, the average heat transfer coefficient decreases. The same behavior can be observed for all heat fluxes studied. The maximum heat transfer coefficient decreases with decreasing heat fluxes.

6. Conclusion

Experiments on flow boiling in small minichannels are carried out and new results are provided. Steady and unsteady behaviors are evidenced and found to be a function of the upstream boundary conditions. A critical Reynolds number is found to delimit steady and unsteady states behaviors in the diagram $\Delta P = f(Re_{IN})$. Two types of unsteady behaviors due to confinement and compliant effects have been detailed and analyzed. They evidence coupling effects between the minichannel and damper in the unsteady regime characterized by pressure loss fluctuations with high amplitudes ($2 < \widetilde{P}/\overline{\Delta P} < 8$) and oscillation frequencies depending on the operating conditions which vary between 3 and 4 Hz. The results obtained differ from those for flow boiling in larger tubes. When a compliant source is provided, the unsteady state regime does not match with the Ledinegg criterion. Furthermore, when the damper is not connected, the flow boiling is still found to be unsteady with different flow patterns and fluctuation characteristics. The pressure loss fluctuations present relatively small amplitudes ($0.25 < \widetilde{P}/\overline{\Delta P} \leqslant 3$) and higher frequencies between 6 and 18 Hz. The average heat transfer coefficient is found to have a maximum value when the unsteady state regime appears, whatever the heat flux provided. The two-phase flow modeling shows a good agreement for the steady state flow boiling. The explanation of the two-phase flow confined fluctuation is currently under investigation.

Acknowledgements

We thank the "Centre National d'Etudes Spatiales" for its financial assistance: grant no. 793/2000/CNES/8308.

Appendix A. Pressure loss modeling

A.1. Basic equations and assumptions

Three equations will be used in this section: the mass conservation equation (A.1), the momentum balance equation (A.2) and the energy balance equation (A.3) applied in a steady state for a one-dimensional geometry and for constant physical properties in the liquid and the vapor zones. The phase change temperature, also called the saturation temperature, is physically a function of pressure but will be considered to be constant in the homogeneous flow assuming low overpressure. The heat flux (Q) supplied to the minichannel is assumed to be constant but it is non-uniform.

$$\frac{\partial \rho}{\partial t} + \frac{\partial(\rho U)}{\partial z} = 0 \tag{A.1}$$

$$\rho\left(\frac{\partial U}{\partial t} + U\frac{\partial U}{\partial z}\right) + F_R[U,z] + \frac{\partial P}{\partial z} + \rho g = 0 \tag{A.2}$$

$$\rho\frac{\partial H}{\partial t} + \rho U\frac{\partial H}{\partial z} = \frac{\partial P}{\partial t} + U\frac{\partial P}{\partial z} + UF_R[U,z] + Q \tag{A.3}$$

F_R is the fluid friction force which can be easily defined for the liquid and the vapor zone. For the homogeneous medium, the friction term is obtained with the two-phase multiplier, also called the Lockart-Martinnelli coefficient; we apply this coefficient to the liquid flow.

Q is the power provided to the minichannel per unit length and per unit of minichannel cross-section. It can be expressed in a steady state as in Eq. (A.4).

$$Q = \frac{q_W(d+2e)}{S_H} \tag{A.4}$$

The mass conservation equation (A.1) in a steady state means that the liquid and vapor velocities in the liquid and vapor zone respectively are constant. The two-phase flow velocity varies between the two like the physical properties: the volumetric mass and kinematic viscosity. In the further equations, we indicate the function parameter as z.

In the steady state and with our boundary conditions Eqs. (A.1)–(A.3) are simplified and coupled and that give

- for the liquid zone (Eqs. (A.5)–(A.7)):

$$\frac{\partial U_L}{\partial z} = 0 \tag{A.5}$$

$$\frac{\partial P_L[z]}{\partial z} = -\rho_L g - \frac{\rho_L U_L^2 \lambda[Re_L]}{2D_H} \tag{A.6}$$

$$\rho_L U_L C_{p_L}\frac{\partial T_L[z]}{\partial z} = U_L\frac{\partial P_L[z]}{\partial z} + \frac{\rho_L U_L^3 \lambda[Re_L]}{2D_H} + \frac{q_W(d+2e)}{S_H} \tag{A.7}$$

- for the homogeneous zone (Eqs. (A.8)–(A.10)):

$$\frac{\partial(\rho_B[z]U_B[z])}{\partial z}=0 \tag{A.8}$$

$$\rho_B[z]U_B[z]\frac{\partial U_B[z]}{\partial z}+\frac{\partial P_B[z]}{\partial z} = -\rho_B[z]g-\frac{\phi^2[z]\rho_L U_L^2\lambda[Re_L]}{2D_H} \tag{A.9}$$

$$U_B[z]\frac{\partial P_B[z]}{\partial z}+U_B[z]\frac{\rho_L U_L^2\phi^2[z]\lambda[Re_L]}{2D_H} +\frac{q_W(d+2e)}{S_H}=\rho_B[z]U_B[z]L_V\frac{\chi[z]}{\partial z} \tag{A.10}$$

- for the vapor zone (Eqs. (A.11)–(A.13)):

$$\frac{\partial U_V}{\partial z}=0 \tag{A.11}$$

$$\frac{\partial P_V[z]}{\partial z}=-\rho_V g-\frac{\rho_V U_V^2\lambda[Re_V]}{2D_H} \tag{A.12}$$

$$\rho_V U_V C_{pv}\frac{\partial T_V[z]}{\partial z}=U_V\frac{\partial P_V[z]}{\partial z}+\frac{\rho_V U_V^3\lambda[Re_V]}{2D_H} +\frac{q_W(d+2e)}{S_H} \tag{A.13}$$

A.2. Definitions

We define the liquid and vapor Reynolds numbers with Eq. A.14(a) and A.14(b) respectively. The vapor velocity in the vapor flow is given by the mass conservation equation. The mass introduced into the inlet must be maintained in the minichannel outlet. Such a conservation law gives Eq. (A.15).

$$Re_L=\frac{U_L D_H}{\nu_L}\quad(a)\quad Re_V=\frac{U_V D_H}{\nu_V}\quad(b) \tag{A.14}$$

$$U_V=\frac{\rho_L}{\rho_V}U_L \tag{A.15}$$

To calculate the minichannel pressure loss, we need the different zone lengths. The subcooling length is obtained by replacing $\frac{\partial P_L}{\partial z}$ from Eq. (A.6) into Eq. (A.7). Z_L, which defines the beginning of the boiling zone, is given by Eq. (A.16).

$$Z_L=\frac{S_H C_{pL}\rho_L U_L(T_{SAT}-T_{IN})}{q_W(d+2e)} \tag{A.16}$$

Z_V, which is the location of vapor quality equal to 1, i.e., the beginning of the vapor flow, is obtained using the latent heat of the phase change. The two-phase flow length is obtained by the energy balance (Eq. (A.17)) between the heat provided to the minichannel and the latent heat necessary to be wholly vapor, the kinetic energy to reach the vapor velocity and the potential energy to reach the minichannel exit.

$$\frac{q_W(d+2e)}{S_H}=\rho_L U_L\frac{\partial(\chi[z]L_V+\frac{1}{2}U^2[z]+gz)}{\partial z} \tag{A.17}$$

Integrated between the end and the beginning of the two-phase flow, Z_V is obtained after simplification: the liquid velocity and gravitational terms are neglected compared with the latent heat of vaporization. Z_V is so given by Eq. (A.18).

$$Z_V=Z_L+\frac{\rho_L U_L S_H}{q_W(d+2e)}\left(L_V+\frac{1}{2}U_V^2\right) \tag{A.18}$$

To be able to calculate the total minichannel pressure loss for all liquid inlet velocities, two lengths are defined following the zones present in the minichannel. L_1 is used to define the end of the liquid zone, which can be either the end of the minichannel if the liquid temperature did not reach the saturation temperature or Z_L as defined previously. L_2 is used to define the end of the two-phase flow zone, which can be either the end of the minichannel if the vapor quality is not equal to 1 or Z_V as defined previously.

$$L_1=\min[Z_L,L]\quad(a)\quad L_2=\min[Z_V,L]\quad(b) \tag{A.19}$$

A.3. Liquid flow pressure loss

The liquid flow pressure loss is determined by the integration of Eq. (A.6) between the liquid zone limits, i.e., the minichannel entrance and L_1. The pressure loss expression is given by Eq. (A.20).

$$\Delta P_L=\left(\rho_L g+\frac{\rho_L}{2D_H}\lambda[Re_L]U_L^2\right)L_1 \tag{A.20}$$

The friction factor of the fluid flow in the minichannel is needed to obtain the final pressure loss expression. The literature [15] gives correlations for liquid flows in rectangular cross-section minichannels. Our aspect ratio of 1/8 implies a factor 1.3 to apply from the theory in circular tubes for both laminar and turbulent flows.

$$\lambda_{TH}=\begin{cases}\dfrac{83.2}{Re} & \text{if } Re<1187\\ \dfrac{0.41132}{Re^{0.25}} & \text{if } Re>1187\end{cases} \tag{A.21}$$

However, an experimental investigation for our minichannel gives a friction factor of about half that of the theoretical prediction. So a complete friction factor study was conducted to show up the experimental friction factor variation in laminar and turbulent regimes. The experimental results are provided in Fig. 13.

$$\lambda_{EXP}=\begin{cases}\dfrac{46.78}{Re} & \text{if } Re<1527\\ \dfrac{0.05198}{Re^{0.07225}} & \text{if } 1527<Re<4046\\ \dfrac{0.2275}{Re^{0.25}} & \text{if } Re>4046\end{cases} \tag{A.22}$$

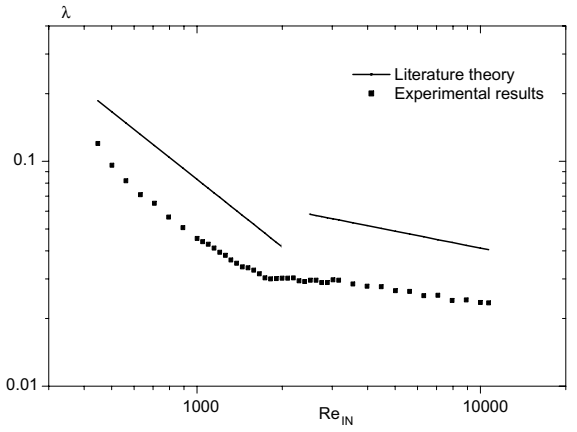

Fig. 13. Minichannel friction factor for Reynolds numbers ranging from 10 to 10,000.

Such differences between the theoretical prediction and the experimental results can be explained in several ways: the small aspect ratio of the minichannel (1/8) which implies a narrow velocity profile in one direction and a wide one in the other direction. Furthermore, in a rectangular geometry the corners are a zone of high gradients which strongly modify the flow field. This experimental friction factor will be used for further computation.

A.4. Homogeneous flow pressure loss

The homogeneous flow velocity is obtained by the spatial integration of Eq. (A.8) between a location in the minichannel (z) and the beginning of the two-phase flow zone. Such equality gives Eq. (A.23) in which the density expression has to be known.

$$U_{\mathrm{B}}[z] = \frac{U_{\mathrm{L}}\rho_{\mathrm{L}}}{\rho_{\mathrm{B}}[z]} \tag{A.23}$$

We provide a constant power to the minichannel, so a constant heat flux is assumed to be provided at the minichannel heating surface. Thus, a linear variation of the vapor quality in the two-phase flow is deduced, which gives Eq. (A.24).

$$\chi[z] = \frac{z - L_1}{Z_{\mathrm{V}} - L_1} \tag{A.24}$$

The void fraction is thus deduced from the vapor quality using a slip velocity model. The model choice is a key point. Physically, the slip ratio evolves as the physical parameters in the homogeneous flow between 1 and $\frac{\rho_{\mathrm{L}}}{\rho_{\mathrm{V}}}$. The model choice will dramatically change the minichannel pressure loss variation. We will use the model defined in Eq. (A.26)(b).

$$\alpha[z] = \frac{\chi[z]\rho_{\mathrm{L}}}{\chi[z]\rho_{\mathrm{L}} + S[z]\rho_{\mathrm{V}}(1-\chi[z])} \tag{A.25}$$

$$S[z] = \begin{cases} 1 & \text{(a) Homogeneous model [16,17]} \\ \left(\frac{\rho_{\mathrm{L}}}{\rho_{\mathrm{V}}}\right)^{1/3} & \text{(b) Zivi model [18]} \\ \left(1+\chi[z]\left(\frac{\rho_{\mathrm{L}}}{\rho_{\mathrm{V}}}-1\right)\right)^{1/2} & \text{(c) Chisholm model [19]} \\ 1+\frac{\rho_{\mathrm{L}}}{\rho_{\mathrm{V}}}\chi[z] & \text{(d) Smith model [17]} \\ \text{CISE correlation} & \text{(e) Premoli model [20]} \end{cases} \tag{A.26}$$

Based on the vapor fraction, we build the density of the homogeneous flow using Eq. (A.27).

$$\rho_{\mathrm{B}}[z] = \alpha[z]\rho_{\mathrm{V}} + (1-\alpha[z])\rho_{\mathrm{L}} \tag{A.27}$$

The homogeneous flow pressure loss is often expressed in terms of a two-phase multiplier. That is the homogeneous pressure loss is equal to a two-phase coefficient multiplied by the single-phase pressure loss for an entire liquid flow (for our situation). Such a two-phase coefficient is given by Eq. (A.28) and is multiplied by the friction factor of an equal total liquid mass flow rate.

$$\phi^2[z] = \frac{1+\frac{\rho_{\mathrm{L}}-\rho_{\mathrm{V}}}{\rho_{\mathrm{V}}}\chi[z]}{\left(1+\frac{\mu_{\mathrm{L}}-\mu_{\mathrm{V}}}{\mu_{\mathrm{V}}}\chi[z]\right)^{1/4}} \tag{A.28}$$

So, the two-phase flow pressure loss can be expressed as using the mass conservation equation by Eq. (A.29):

$$\Delta P_{\mathrm{B}} = -gK_1 - \frac{\rho_{\mathrm{L}}K_2U_{\mathrm{L}}^2\lambda[Re_{\mathrm{L}}]}{2D_{\mathrm{H}}} - \rho_{\mathrm{L}}U_{\mathrm{L}}(U_{\mathrm{B}}[L_2] - U_{\mathrm{L}}) \tag{A.29}$$

with K_1 and K_2 defined in Eq. (A.30) for simplification.

$$K_1 = \int_{L_1}^{L_2} \rho_{\mathrm{B}}[z]\,\mathrm{d}z \ (a) \quad K_2 = \int_{L_1}^{L_2} \phi^2[z]\,\mathrm{d}z \ (b) \tag{A.30}$$

Thus, the total pressure loss becomes the sum of three pressure loss terms called the acceleration term (ΔP_{B1}) defined in Eq. (A.31), the gravitational term (ΔP_{B2}) defined in Eq. (A.32) and the frictional term (ΔP_{B3}) defined in Eq. (A.33).

$$\Delta P_{\mathrm{B1}} = \rho_{\mathrm{L}}U_{\mathrm{L}}(U_{\mathrm{B}}[L_2] - U_{\mathrm{L}}) \tag{A.31}$$

$$\Delta P_{\mathrm{B2}} = gK_1 \tag{A.32}$$

$$\Delta P_{\mathrm{B3}} = \frac{\rho_{\mathrm{L}}}{2D_{\mathrm{H}}}K_2U_{\mathrm{L}}^2\lambda[Re_{\mathrm{L}}] \tag{A.33}$$

A.5. Vapor flow pressure loss

The vapor flow pressure loss is determined by the integration of Eq. (A.12) between the beginning of the vapor zone, i.e. L_2, and the end of the minichannel. The pressure loss expression is given by Eq. (A.34).

$$\Delta P_V = \left(\rho_V g + \frac{\rho_V}{2D_H}\lambda[Re_V]U_V^2\right)(L - L_2) \quad (A.34)$$

A.6. Total minichannel pressure loss

The total minichannel pressure loss is given by Eq. (A.35). This expression includes the liquid, two-phase and vapor pressure loss expressions.

$$\Delta P_T = \Delta P_L + \Delta P_B + \Delta P_V \quad (A.35)$$

It is possible to group each contribution as in the two-phase flow section. It appears the gravitational, inertial and frictional contributions of each zone (Eq. (A.36)).

$$\begin{aligned}\Delta P_T = {} & g[\rho_L L_1 + K_1 + \rho_V(L - L_2)] \\ & + \rho_L U_L(U_B[L_2] - U_L) \\ & + \frac{\rho_L\lambda[Re_L]U_L^2(L_1 + K_2) + \rho_V\lambda[Re_V]U_V^2(L - L_2)}{2D_H}\end{aligned} \quad (A.36)$$

References

[1] M.F. Dowling, S.I. Abdel-Khalik, S.M. Ghiaasiaan, S.M. Jeter, Z.H. Quershi, J.E. Kennedy, G.M. Roach, The onset of flow instability in uniformly heated horizontal micro-minichannels, J. Heat Transfer 122 (2000) 118–125.

[2] S.G. Kandlikar, Fundamental issues related to flow boiling in minichannels and microminichannels, in: Experimental Heat Transfer, Fluid Mechanics, and Thermodynamics—ExHFT-5, vol. 1, Edizioni ETS, Pisa, September 2001, pp. 129–146.

[3] D. Wen, D.B.R. Kenning, Y. Yan, Flow boiling of water in a narrow vertical minichannel at low mass flux: observations of local phenomena, in: Proc. IHTC 12, Grenoble, France, 2002.

[4] M. Ledinegg, Instability flow during natural forced circulation, Warme 61 (8) (1938) 891–898.

[5] P.A. Kew, K. Cornwell, Confined bubble flow and boiling in narrow spaces, in: Proc. IHTC 10, Brighton 7, 1994, pp. 473–478.

[6] P.A. Kew, K. Cornwell, On pressure fluctuations during boiling in narrow minichannels, in: 2nd European Thermal-Sciences and 14th UIT National Heat Transfer Conference, 1996, pp. 1323–1327.

[7] M. Aligoodarz, Y. Yan, D. Kenning, Wall temperature and pressure variations during flow boiling in narrow minichannels, in: Proc. IHTC 11, Kyongju, Korea, vol. 2, 1998, pp. 225–230.

[8] B.X. Wang, X.F. Peng, Forced-convection and boiling characteristics in microminichannels, in: Proc. IHTC 11, Kyongju, Korea, 1998, pp. 371–390.

[9] Y. Zohar, L. Jiang, M. Wong, Phase change in microminichannel heat sink under forced convection boiling, in: 13th Annual International Workshop on Micro Electro Mechanical Systems, 2000, pp. 397–402.

[10] D. Yu, R. Warrington, R. Barron, T. Ameel, An experimental and theoretical investigation of fluid flow and heat transfer in microtubes, in: Proc. ASME/JSME Thermal Engineering Joint Conference, Hawai, vol. 1, 1995, pp. 523–530.

[11] D. Brutin, F. Topin, L. Tadrist, Experimental study of the unsteady convective boiling in heated minichannels, Int. J. Heat Mass Transfer 46 (16) (2003) 2957–2965.

[12] D. Brutin, F. Topin, L. Tadrist, On thermo-hydraulic instabilities in small minichannels during flow boiling, in: Experimental Heat Transfer, Fluid Mechanics and Thermodynamics Conference, Thessaloniki, Greece, vol. 1, 2001, pp. 273–277.

[13] A. Mihaila, J.A. Bouré, The oscillatory behavior of heated minichannels, in: Symp. on Two-phase Flow Dynamics, Eindhoven, September 1967, pp. 695–720.

[14] G.M. Callahan, A.H. Stenning, T.N. Veziroglu, Pressure drop oscillations in forced convection flow with boiling, in: Symp. on Two-phase Flow Dynamics, Eindhoven, vol. 1, September 1967, pp. 405–427.

[15] I.E. Idel'cik, Memento des pertes de charge, in: Collection de la Direction des Etudes et Recherches d'Electricités de France, 1969, pp. 55–89 (Chapter 2).

[16] P.B. Whalley, Boiling Condensation and Gas–Liquid Flow, Oxford Science Publications, 1987.

[17] V.P. Carey, Liquid–Vapor Phase Change Phenomena, Taylor & Francis, 1984.

[18] S.M. Zivi, Estimation of steady-state steam void fraction by means of the principle of minimum entropy production, Trans. ASME—J. Heat Transfer 86 (1964) 247–252.

[19] D. Chisholm, An equation for velocity ratio in two-phase flow, NEL Report 535, 1972.

[20] A. Premoli, D. Francesco, A. Prina, An empirical correlation for evaluating two-phase mixture density under adiabatic conditions, in: European Two-phase Flow Group Meeting, Milan, 1970.